March 2008

BABAR-PUB-07/073
SLAC-PUB-13160

Measurement of the Spin of the $\Xi(1530)$ Resonance

B. Aubert,[1] M. Bona,[1] Y. Karyotakis,[1] J. P. Lees,[1] V. Poireau,[1] X. Prudent,[1] V. Tisserand,[1] A. Zghiche,[1] J. Garra Tico,[2] E. Grauges,[2] L. Lopez,[3] A. Palano,[3] M. Pappagallo,[3] G. Eigen,[4] B. Stugu,[4] L. Sun,[4] G. S. Abrams,[5] M. Battaglia,[5] D. N. Brown,[5] J. Button-Shafer,[5] R. N. Cahn,[5] R. G. Jacobsen,[5] J. A. Kadyk,[5] L. T. Kerth,[5] Yu. G. Kolomensky,[5] G. Kukartsev,[5] G. Lynch,[5] I. L. Osipenkov,[5] M. T. Ronan,[5,*] K. Tackmann,[5] T. Tanabe,[5] W. A. Wenzel,[5] C. M. Hawkes,[6] N. Soni,[6] A. T. Watson,[6] H. Koch,[7] T. Schroeder,[7] D. Walker,[8] D. J. Asgeirsson,[9] T. Cuhadar-Donszelmann,[9] B. G. Fulsom,[9] C. Hearty,[9] T. S. Mattison,[9] J. A. McKenna,[9] M. Barrett,[10] A. Khan,[10] M. Saleem,[10] L. Teodorescu,[10] V. E. Blinov,[11] A. D. Bukin,[11] A. R. Buzykaev,[11] V. P. Druzhinin,[11] V. B. Golubev,[11] A. P. Onuchin,[11] S. I. Serednyakov,[11] Yu. I. Skovpen,[11] E. P. Solodov,[11] K. Yu. Todyshev,[11] M. Bondioli,[12] S. Curry,[12] I. Eschrich,[12] D. Kirkby,[12] A. J. Lankford,[12] P. Lund,[12] M. Mandelkern,[12] E. C. Martin,[12] D. P. Stoker,[12] S. Abachi,[13] C. Buchanan,[13] J. W. Gary,[14] F. Liu,[14] O. Long,[14] B. C. Shen,[14,*] G. M. Vitug,[14] Z. Yasin,[14] L. Zhang,[14] H. P. Paar,[15] S. Rahatlou,[15] V. Sharma,[15] C. Campagnari,[16] T. M. Hong,[16] D. Kovalskyi,[16] M. A. Mazur,[16] J. D. Richman,[16] T. W. Beck,[17] A. M. Eisner,[17] C. J. Flacco,[17] C. A. Heusch,[17] J. Kroseberg,[17] W. S. Lockman,[17] T. Schalk,[17] B. A. Schumm,[17] A. Seiden,[17] M. G. Wilson,[17] L. O. Winstrom,[17] E. Chen,[18] C. H. Cheng,[18] D. A. Doll,[18] B. Echenard,[18] F. Fang,[18] D. G. Hitlin,[18] I. Narsky,[18] T. Piatenko,[18] F. C. Porter,[18] R. Andreassen,[19] G. Mancinelli,[19] B. T. Meadows,[19] K. Mishra,[19] M. D. Sokoloff,[19] F. Blanc,[20] P. C. Bloom,[20] W. T. Ford,[20] J. F. Hirschauer,[20] A. Kreisel,[20] M. Nagel,[20] U. Nauenberg,[20] A. Olivas,[20] J. G. Smith,[20] K. A. Ulmer,[20] S. R. Wagner,[20] R. Ayad,[21,†] A. M. Gabareen,[21] A. Soffer,[21,‡] W. H. Toki,[21] R. J. Wilson,[21] D. D. Altenburg,[22] E. Feltresi,[22] A. Hauke,[22] H. Jasper,[22] M. Karbach,[22] J. Merkel,[22] A. Petzold,[22] B. Spaan,[22] K. Wacker,[22] V. Klose,[23] M. J. Kobel,[23] H. M. Lacker,[23] W. F. Mader,[23] R. Nogowski,[23] J. Schubert,[23] K. R. Schubert,[23] R. Schwierz,[23] J. E. Sundermann,[23] A. Volk,[23] D. Bernard,[24] G. R. Bonneaud,[24] E. Latour,[24] Ch. Thiebaux,[24] M. Verderi,[24] P. J. Clark,[25] W. Gradl,[25] S. Playfer,[25] A. I. Robertson,[25] J. E. Watson,[25] M. Andreotti,[26] D. Bettoni,[26] C. Bozzi,[26] R. Calabrese,[26] A. Cecchi,[26] G. Cibinetto,[26] P. Franchini,[26] E. Luppi,[26] M. Negrini,[26] A. Petrella,[26] L. Piemontese,[26] E. Prencipe,[26] V. Santoro,[26] F. Anulli,[27] R. Baldini-Ferroli,[27] A. Calcaterra,[27] R. de Sangro,[27] G. Finocchiaro,[27] S. Pacetti,[27] P. Patteri,[27] I. M. Peruzzi,[27,§] M. Piccolo,[27] M. Rama,[27] A. Zallo,[27] A. Buzzo,[28] R. Contri,[28] M. Lo Vetere,[28] M. M. Macri,[28] M. R. Monge,[28] S. Passaggio,[28] C. Patrignani,[28] E. Robutti,[28] A. Santroni,[28] S. Tosi,[28] K. S. Chaisanguanthum,[29] M. Morii,[29] R. S. Dubitzky,[30] J. Marks,[30] S. Schenk,[30] U. Uwer,[30] D. J. Bard,[31] P. D. Dauncey,[31] J. A. Nash,[31] W. Panduro Vazquez,[31] M. Tibbetts,[31] P. K. Behera,[32] X. Chai,[32] M. J. Charles,[32] U. Mallik,[32] J. Cochran,[33] H. B. Crawley,[33] L. Dong,[33] V. Eyges,[33] W. T. Meyer,[33] S. Prell,[33] E. I. Rosenberg,[33] A. E. Rubin,[33] Y. Y. Gao,[34] A. V. Gritsan,[34] Z. J. Guo,[34] C. K. Lae,[34] A. G. Denig,[35] M. Fritsch,[35] G. Schott,[35] N. Arnaud,[36] J. Béquilleux,[36] A. D'Orazio,[36] M. Davier,[36] J. Firmino da Costa,[36] G. Grosdidier,[36] A. Höcker,[36] V. Lepeltier,[36] F. Le Diberder,[36] A. M. Lutz,[36] S. Pruvot,[36] P. Roudeau,[36] M. H. Schune,[36] J. Serrano,[36] V. Sordini,[36] A. Stocchi,[36] W. F. Wang,[36] G. Wormser,[36] D. J. Lange,[37] D. M. Wright,[37] I. Bingham,[38] J. P. Burke,[38] C. A. Chavez,[38] J. R. Fry,[38] E. Gabathuler,[38] R. Gamet,[38] D. E. Hutchcroft,[38] D. J. Payne,[38] C. Touramanis,[38] A. J. Bevan,[39] K. A. George,[39] F. Di Lodovico,[39] R. Sacco,[39] M. Sigamani,[39] G. Cowan,[40] H. U. Flaecher,[40] D. A. Hopkins,[40] S. Paramesvaran,[40] F. Salvatore,[40] A. C. Wren,[40] D. N. Brown,[41] C. L. Davis,[41] K. E. Alwyn,[42] N. R. Barlow,[42] R. J. Barlow,[42] Y. M. Chia,[42] C. L. Edgar,[42] G. D. Lafferty,[42] T. J. West,[42] J. I. Yi,[42] J. Anderson,[43] C. Chen,[43] A. Jawahery,[43] D. A. Roberts,[43] G. Simi,[43] J. M. Tuggle,[43] C. Dallapiccola,[44] S. S. Hertzbach,[44] X. Li,[44] E. Salvati,[44] S. Saremi,[44] R. Cowan,[45] D. Dujmic,[45] P. H. Fisher,[45] K. Koeneke,[45] G. Sciolla,[45] M. Spitznagel,[45] F. Taylor,[45] R. K. Yamamoto,[45] M. Zhao,[45] S. E. Mclachlin,[46,*] P. M. Patel,[46] S. H. Robertson,[46] A. Lazzaro,[47] V. Lombardo,[47] F. Palombo,[47] J. M. Bauer,[48] L. Cremaldi,[48] V. Eschenburg,[48] R. Godang,[48] R. Kroeger,[48] D. A. Sanders,[48] D. J. Summers,[48] H. W. Zhao,[48] S. Brunet,[49] D. Côté,[49] M. Simard,[49] P. Taras,[49] F. B. Viaud,[49] H. Nicholson,[50] G. De Nardo,[51] L. Lista,[51] D. Monorchio,[51] C. Sciacca,[51] M. A. Baak,[52] G. Raven,[52] H. L. Snoek,[52] C. P. Jessop,[53] K. J. Knoepfel,[53] J. M. LoSecco,[53] G. Benelli,[54] L. A. Corwin,[54] K. Honscheid,[54] H. Kagan,[54] R. Kass,[54] J. P. Morris,[54] A. M. Rahimi,[54] J. J. Regensburger,[54] S. J. Sekula,[54] Q. K. Wong,[54] N. L. Blount,[55] J. Brau,[55] R. Frey,[55] O. Igonkina,[55] J. A. Kolb,[55] M. Lu,[55] R. Rahmat,[55] N. B. Sinev,[55] D. Strom,[55] J. Strube,[55] E. Torrence,[55] G. Castelli,[56] N. Gagliardi,[56] A. Gaz,[56] M. Margoni,[56] M. Morandin,[56] M. Posocco,[56] M. Rotondo,[56] F. Simonetto,[56] R. Stroili,[56] C. Voci,[56] P. del Amo Sanchez,[57] E. Ben-Haim,[57] H. Briand,[57] G. Calderini,[57] J. Chauveau,[57] P. David,[57] L. Del Buono,[57] O. Hamon,[57] Ph. Leruste,[57] J. Malclès,[57] J. Ocariz,[57] A. Perez,[57] J. Prendki,[57] L. Gladney,[58] M. Biasini,[59] R. Covarelli,[59] E. Manoni,[59] C. Angelini,[60] G. Batignani,[60] S. Bettarini,[60] M. Carpinelli,[60,¶] A. Cervelli,[60] F. Forti,[60] M. A. Giorgi,[60] A. Lusiani,[60] G. Marchiori,[60] M. Morganti,[60] N. Neri,[60] E. Paoloni,[60] G. Rizzo,[60] J. J. Walsh,[60] J. Biesiada,[61] Y. P. Lau,[61] D. Lopes Pegna,[61] C. Lu,[61]

Submitted to Physical Review D

Work supported in part by US Department of Energy contract DE-AC02-76SF00515

J. Olsen,[61] A. J. S. Smith,[61] A. V. Telnov,[61] E. Baracchini,[62] G. Cavoto,[62] D. del Re,[62] E. Di Marco,[62] R. Faccini,[62] F. Ferrarotto,[62] F. Ferroni,[62] M. Gaspero,[62] P. D. Jackson,[62] M. A. Mazzoni,[62] S. Morganti,[62] G. Piredda,[62] F. Polci,[62] F. Renga,[62] C. Voena,[62] M. Ebert,[63] T. Hartmann,[63] H. Schröder,[63] R. Waldi,[63] T. Adye,[64] B. Franek,[64] E. O. Olaiya,[64] W. Roethel,[64] F. F. Wilson,[64] S. Emery,[65] M. Escalier,[65] A. Gaidot,[65] S. F. Ganzhur,[65] G. Hamel de Monchenault,[65] W. Kozanecki,[65] G. Vasseur,[65] Ch. Yèche,[65] M. Zito,[65] X. R. Chen,[66] H. Liu,[66] W. Park,[66] M. V. Purohit,[66] R. M. White,[66] J. R. Wilson,[66] M. T. Allen,[67] D. Aston,[67] R. Bartoldus,[67] P. Bechtle,[67] J. F. Benitez,[67] R. Cenci,[67] J. P. Coleman,[67] M. R. Convery,[67] J. C. Dingfelder,[67] J. Dorfan,[67] G. P. Dubois-Felsmann,[67] W. Dunwoodie,[67] R. C. Field,[67] T. Glanzman,[67] S. J. Gowdy,[67] M. T. Graham,[67] P. Grenier,[67] C. Hast,[67] W. R. Innes,[67] J. Kaminski,[67] M. H. Kelsey,[67] H. Kim,[67] P. Kim,[67] M. L. Kocian,[67] D. W. G. S. Leith,[67] S. Li,[67] B. Lindquist,[67] S. Luitz,[67] V. Luth,[67] H. L. Lynch,[67] D. B. MacFarlane,[67] H. Marsiske,[67] R. Messner,[67] D. R. Muller,[67] H. Neal,[67] S. Nelson,[67] C. P. O'Grady,[67] I. Ofte,[67] A. Perazzo,[67] M. Perl,[67] B. N. Ratcliff,[67] A. Roodman,[67] A. A. Salnikov,[67] R. H. Schindler,[67] J. Schwiening,[67] A. Snyder,[67] D. Su,[67] M. K. Sullivan,[67] K. Suzuki,[67] S. K. Swain,[67] J. M. Thompson,[67] J. Va'vra,[67] A. P. Wagner,[67] M. Weaver,[67] W. J. Wisniewski,[67] M. Wittgen,[67] D. H. Wright,[67] H. W. Wulsin,[67] A. K. Yarritu,[67] K. Yi,[67] C. C. Young,[67] V. Ziegler,[67] P. R. Burchat,[68] A. J. Edwards,[68] S. A. Majewski,[68] T. S. Miyashita,[68] B. A. Petersen,[68] L. Wilden,[68] S. Ahmed,[69] M. S. Alam,[69] R. Bula,[69] J. A. Ernst,[69] B. Pan,[69] M. A. Saeed,[69] S. B. Zain,[69] S. M. Spanier,[70] B. J. Wogsland,[70] R. Eckmann,[71] J. L. Ritchie,[71] A. M. Ruland,[71] C. J. Schilling,[71] R. F. Schwitters,[71] J. M. Izen,[72] X. C. Lou,[72] S. Ye,[72] F. Bianchi,[73] D. Gamba,[73] M. Pelliccioni,[73] M. Bomben,[74] L. Bosisio,[74] C. Cartaro,[74] F. Cossutti,[74] G. Della Ricca,[74] L. Lanceri,[74] L. Vitale,[74] V. Azzolini,[75] N. Lopez-March,[75] F. Martinez-Vidal,[75] D. A. Milanes,[75] A. Oyanguren,[75] J. Albert,[76] Sw. Banerjee,[76] B. Bhuyan,[76] K. Hamano,[76] R. Kowalewski,[76] I. M. Nugent,[76] J. M. Roney,[76] R. J. Sobie,[76] T. J. Gershon,[77] P. F. Harrison,[77] J. Ilic,[77] T. E. Latham,[77] G. B. Mohanty,[77] H. R. Band,[78] X. Chen,[78] S. Dasu,[78] K. T. Flood,[78] P. E. Kutter,[78] Y. Pan,[78] M. Pierini,[78] R. Prepost,[78] C. O. Vuosalo,[78] and S. L. Wu[78]

(The *BABAR* Collaboration)

[1] *Laboratoire de Physique des Particules, IN2P3/CNRS et Université de Savoie, F-74941 Annecy-Le-Vieux, France*
[2] *Universitat de Barcelona, Facultat de Fisica, Departament ECM, E-08028 Barcelona, Spain*
[3] *Università di Bari, Dipartimento di Fisica and INFN, I-70126 Bari, Italy*
[4] *University of Bergen, Institute of Physics, N-5007 Bergen, Norway*
[5] *Lawrence Berkeley National Laboratory and University of California, Berkeley, California 94720, USA*
[6] *University of Birmingham, Birmingham, B15 2TT, United Kingdom*
[7] *Ruhr Universität Bochum, Institut für Experimentalphysik 1, D-44780 Bochum, Germany*
[8] *University of Bristol, Bristol BS8 1TL, United Kingdom*
[9] *University of British Columbia, Vancouver, British Columbia, Canada V6T 1Z1*
[10] *Brunel University, Uxbridge, Middlesex UB8 3PH, United Kingdom*
[11] *Budker Institute of Nuclear Physics, Novosibirsk 630090, Russia*
[12] *University of California at Irvine, Irvine, California 92697, USA*
[13] *University of California at Los Angeles, Los Angeles, California 90024, USA*
[14] *University of California at Riverside, Riverside, California 92521, USA*
[15] *University of California at San Diego, La Jolla, California 92093, USA*
[16] *University of California at Santa Barbara, Santa Barbara, California 93106, USA*
[17] *University of California at Santa Cruz, Institute for Particle Physics, Santa Cruz, California 95064, USA*
[18] *California Institute of Technology, Pasadena, California 91125, USA*
[19] *University of Cincinnati, Cincinnati, Ohio 45221, USA*
[20] *University of Colorado, Boulder, Colorado 80309, USA*
[21] *Colorado State University, Fort Collins, Colorado 80523, USA*
[22] *Universität Dortmund, Institut für Physik, D-44221 Dortmund, Germany*
[23] *Technische Universität Dresden, Institut für Kern- und Teilchenphysik, D-01062 Dresden, Germany*
[24] *Laboratoire Leprince-Ringuet, CNRS/IN2P3, Ecole Polytechnique, F-91128 Palaiseau, France*
[25] *University of Edinburgh, Edinburgh EH9 3JZ, United Kingdom*
[26] *Università di Ferrara, Dipartimento di Fisica and INFN, I-44100 Ferrara, Italy*
[27] *Laboratori Nazionali di Frascati dell'INFN, I-00044 Frascati, Italy*
[28] *Università di Genova, Dipartimento di Fisica and INFN, I-16146 Genova, Italy*
[29] *Harvard University, Cambridge, Massachusetts 02138, USA*
[30] *Universität Heidelberg, Physikalisches Institut, Philosophenweg 12, D-69120 Heidelberg, Germany*
[31] *Imperial College London, London, SW7 2AZ, United Kingdom*
[32] *University of Iowa, Iowa City, Iowa 52242, USA*
[33] *Iowa State University, Ames, Iowa 50011-3160, USA*
[34] *Johns Hopkins University, Baltimore, Maryland 21218, USA*
[35] *Universität Karlsruhe, Institut für Experimentelle Kernphysik, D-76021 Karlsruhe, Germany*

[36] Laboratoire de l'Accélérateur Linéaire, IN2P3/CNRS et Université Paris-Sud 11, Centre Scientifique d'Orsay, B. P. 34, F-91898 ORSAY Cedex, France
[37] Lawrence Livermore National Laboratory, Livermore, California 94550, USA
[38] University of Liverpool, Liverpool L69 7ZE, United Kingdom
[39] Queen Mary, University of London, E1 4NS, United Kingdom
[40] University of London, Royal Holloway and Bedford New College, Egham, Surrey TW20 0EX, United Kingdom
[41] University of Louisville, Louisville, Kentucky 40292, USA
[42] University of Manchester, Manchester M13 9PL, United Kingdom
[43] University of Maryland, College Park, Maryland 20742, USA
[44] University of Massachusetts, Amherst, Massachusetts 01003, USA
[45] Massachusetts Institute of Technology, Laboratory for Nuclear Science, Cambridge, Massachusetts 02139, USA
[46] McGill University, Montréal, Québec, Canada H3A 2T8
[47] Università di Milano, Dipartimento di Fisica and INFN, I-20133 Milano, Italy
[48] University of Mississippi, University, Mississippi 38677, USA
[49] Université de Montréal, Physique des Particules, Montréal, Québec, Canada H3C 3J7
[50] Mount Holyoke College, South Hadley, Massachusetts 01075, USA
[51] Università di Napoli Federico II, Dipartimento di Scienze Fisiche and INFN, I-80126, Napoli, Italy
[52] NIKHEF, National Institute for Nuclear Physics and High Energy Physics, NL-1009 DB Amsterdam, The Netherlands
[53] University of Notre Dame, Notre Dame, Indiana 46556, USA
[54] Ohio State University, Columbus, Ohio 43210, USA
[55] University of Oregon, Eugene, Oregon 97403, USA
[56] Università di Padova, Dipartimento di Fisica and INFN, I-35131 Padova, Italy
[57] Laboratoire de Physique Nucléaire et de Hautes Energies, IN2P3/CNRS, Université Pierre et Marie Curie-Paris6, Université Denis Diderot-Paris7, F-75252 Paris, France
[58] University of Pennsylvania, Philadelphia, Pennsylvania 19104, USA
[59] Università di Perugia, Dipartimento di Fisica and INFN, I-06100 Perugia, Italy
[60] Università di Pisa, Dipartimento di Fisica, Scuola Normale Superiore and INFN, I-56127 Pisa, Italy
[61] Princeton University, Princeton, New Jersey 08544, USA
[62] Università di Roma La Sapienza, Dipartimento di Fisica and INFN, I-00185 Roma, Italy
[63] Universität Rostock, D-18051 Rostock, Germany
[64] Rutherford Appleton Laboratory, Chilton, Didcot, Oxon, OX11 0QX, United Kingdom
[65] DSM/Dapnia, CEA/Saclay, F-91191 Gif-sur-Yvette, France
[66] University of South Carolina, Columbia, South Carolina 29208, USA
[67] Stanford Linear Accelerator Center, Stanford, California 94309, USA
[68] Stanford University, Stanford, California 94305-4060, USA
[69] State University of New York, Albany, New York 12222, USA
[70] University of Tennessee, Knoxville, Tennessee 37996, USA
[71] University of Texas at Austin, Austin, Texas 78712, USA
[72] University of Texas at Dallas, Richardson, Texas 75083, USA
[73] Università di Torino, Dipartimento di Fisica Sperimentale and INFN, I-10125 Torino, Italy
[74] Università di Trieste, Dipartimento di Fisica and INFN, I-34127 Trieste, Italy
[75] IFIC, Universitat de Valencia-CSIC, E-46071 Valencia, Spain
[76] University of Victoria, Victoria, British Columbia, Canada V8W 3P6
[77] Department of Physics, University of Warwick, Coventry CV4 7AL, United Kingdom
[78] University of Wisconsin, Madison, Wisconsin 53706, USA

(Dated: March 12, 2008)

The properties of the $\Xi(1530)$ resonance are investigated in the $\Lambda_c^+ \to \Xi^-\pi^+K^+$ decay process. The data sample was collected with the *BABAR* detector at the SLAC PEP-II asymmetric-energy e^+e^- collider operating at center of mass energies 10.58 and 10.54 GeV. The corresponding integrated luminosity is approximately 230 fb^{-1}. The spin of the $\Xi(1530)$ is established to be 3/2. The existence of an S-wave amplitude in the $\Xi^-\pi^+$ system is inferred, and its interference with the $\Xi(1530)^0$ amplitude provides the first clear demonstration of the Breit-Wigner phase motion expected for the $\Xi(1530)$. The $P_1(\cos\theta_{\Xi^-})$ Legendre polynomial moment indicates the presence of a significant S-wave amplitude for $\Xi^-\pi^+$ mass values above 1.6 GeV/c^2, and a dip in the mass distribution at approximately 1.7 GeV/c^2 is interpreted as due to coherent addition of a $\Xi(1690)^0$ contribution to this amplitude. This would imply $J^P = 1/2^-$ for the $\Xi(1690)$. Attempts at fitting the $\Xi(1530)^0$ lineshape yield unsatisfactory results, and this failure is attributed to interference effects associated with the amplitudes describing the $K^+\pi^+$ and/or Ξ^-K^+ systems.

PACS numbers: 13.30.Eg,14.20.Jn,14.20.Lq

*Deceased

†Now at Temple University, Philadelphia, PA 19122, USA

I. INTRODUCTION

The $\Xi(1530)$ is the only cascade resonance whose properties are reasonably well understood. It decays $\sim 100\%$ to $\Xi\pi$ and $< 4\%$ to $\Xi\gamma$ [1], and its mass (PDG fit: $m(\Xi(1530)^0) = 1531.80 \pm 0.32\,\mathrm{MeV/c^2}$) and width (PDG fit: $\Gamma(\Xi(1530)^0) = 0.1 \pm 0.5$ MeV/c) are reasonably well known [1]. A spin-parity analysis of data on the reactions $K^- p \to \Xi(1530)^{0,-} K^{0,+}$ carried out by Schlein et *al.* [2] showed that $J^P = 3/2^+$ (i.e., P-wave) or $J^P = 5/2^-$ (i.e., D-wave) is favored, and that the data are consistent with $J \geq 3/2$; however, they stated that spin $> 3/2$ is not required, and on this basis concluded that $J^P = 3/2^+$. This conclusion was supported by Button-Schafer et *al.* [3] in a similar analysis. Both experiments ruled out $J = 1/2$, but the claim that $J > 3/2$ was not required was the basis for the conclusion that $J^P = 3/2^+$. In the present paper, the Ω^- spin analysis procedures described in Ref. [4] are extended to the quasi-two-body decay $\Lambda_c^+ \to (\Xi^-\pi^+)K^+$, for which the $\Xi^-\pi^+$ invariant mass distribution exhibits a dominant $\Xi(1530)^0$ signal [5]. Under the assumption that the Λ_c^+ has spin 1/2, it is established that the $\Xi(1530)$ has spin 3/2. On the basis of the analyses of Refs. [2, 3], it follows that positive parity is established.

The data sample and event selection procedures are described in Section II, and the $\Xi(1530)$ spin measurement is presented in Section III. In Section IV, the amplitude structure in the $\Xi(1530)$ region is investigated in some detail, and this is followed by an examination of the $\Xi^-\pi^+$ system at higher mass values in Section V. The unsuccessful attempts at precise measurements of the mass and width of the $\Xi(1530)^0$ are presented in Section VI, and their implications considered. Finally, the conclusions drawn from this analysis are summarized in Section VII.

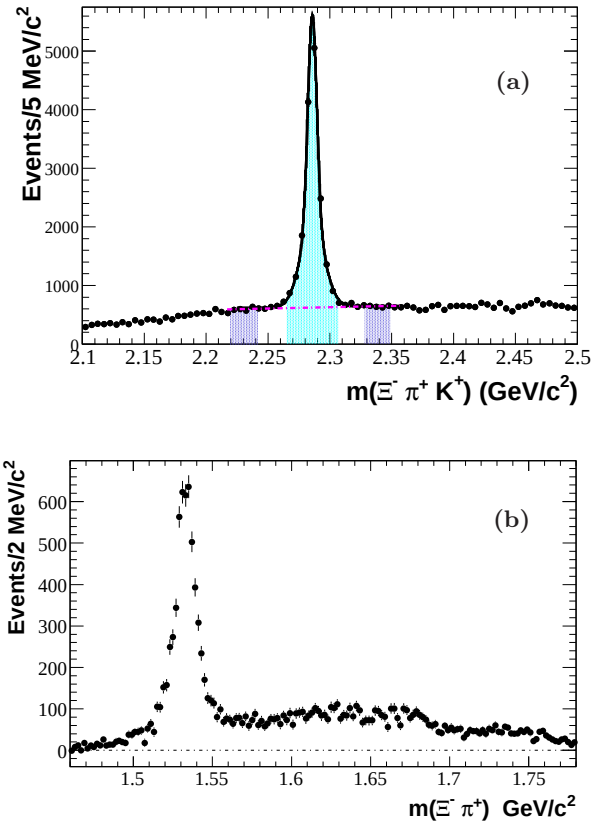

FIG. 1: (a) The uncorrected $\Xi^-\pi^+K^+$ invariant mass spectrum. The curve results from the fit described in the text. The dot-dashed line indicates the fitted background contribution. The shaded areas delimit the signal (light area) and mass-sideband (dark area) regions. (b) The uncorrected Λ_c^+-mass-sideband-subtracted $\Xi^-\pi^+$ invariant mass projection for $\Xi^-\pi^+K^+$ candidates. In each figure, the points with error bars represent the data.

II. THE *BABAR* DETECTOR AND $\Lambda_c^+ \to \Xi^-\pi^+K^+$ EVENT SELECTION

The data sample used for this analysis was collected with the *BABAR* detector at the PEP-II asymmetric-energy e^+e^- collider operating at center-of-mass (c.m.) energies 10.58 and 10.54 GeV, and corresponds to a total integrated luminosity of about 230 fb^{-1}.

Charged particles are detected with a five-layer, double-sided silicon vertex tracker (SVT) and a 40-layer drift chamber (DCH) with a helium-isobutane gas mixture, placed in a 1.5-T solenoidal field produced by a superconducting magnet. The charged-particle momentum resolution is approximately $(\delta p_T/p_T)^2 = (0.0013\,p_T)^2 + (0.0045)^2$, where p_T is the transverse momentum in GeV/c. The SVT, with a typical single-hit resolution of 10 μm, measures the impact parameters of charged-particle tracks in both the plane transverse to the beam direction and along the collision axis.

Charged-particle types are identified from the ionization energy loss (dE/dx) measured in the DCH and SVT, and from the Cherenkov radiation detected in a ring-imaging Cherenkov device. Photons are detected by a CsI(Tl) electromagnetic calorimeter with an energy resolution $\sigma(E)/E = 0.023 \cdot (E/GeV)^{-1/4} \oplus 0.019$.

The return yoke of the superconducting coil is instrumented with resistive plate chambers for the identification and muons and the detection of neutral hadrons. The detector is described in detail in Ref. [6].

The selection of Λ_c^+ candidates requires the intermediate reconstruction of events consistent with $\Xi^- \to \Lambda\,\pi^-$

‡Now at Tel Aviv University, Tel Aviv, 69978, Israel
§Also with Università di Perugia, Dipartimento di Fisica, Perugia, Italy
¶Also with Universita' di Sassari, Sassari, Italy

and $\Lambda \to p\,\pi^-$. Particle identification (PID) selectors based on specific energy loss (dE/dx) and Cherenkov angle measurements are used to identify the proton, pion, and kaon final state tracks [6]. Each intermediate state candidate is required to have invariant mass within a $\pm 3\sigma$ window centered on the fitted peak position of the relevant distribution, where σ is the mass resolution obtained from the fit. A fit is then performed to the complete decay topology with the Λ and Ξ^- candidates constrained to their known mass values [1]. The fit probability is required to be greater than 0.001 in order to ensure simultaneous satisfaction of the topological and mass constraint requirements; this reduces combinatorial background significantly and retains good signal efficiency. Since each weakly-decaying intermediate state (i.e., hyperon) is long-lived, an improvement of the signal-to-background ratio is achieved by requiring that the decay vertex of each hyperon be displaced from its point of origin in the direction of its momentum vector. The distance between the $\Xi^- K^+ \pi^+$ vertex and the Ξ^- decay vertex in the plane perpendicular to the collision axis must exceed 1.5 mm in the Ξ^- direction, and the distance between the Ξ^- and Λ decay vertices must exceed 1.5 mm in the direction of the Λ momentum vector. Finally, the momentum of the Λ_c^+ candidate in the e^+e^- c.m. frame p^* is required to be greater than 2.0 GeV/c, since it is found empirically that this significantly reduces combinatorial background. The invariant mass spectrum of Λ_c^+ candidates which satisfy these selection criteria before efficiency correction is shown in Fig. 1(a). A signal yield of 13035 ± 163 events is obtained from a fit which makes use of a signal function consisting of two Gaussians with a common center and a linear background function to the mass region 2.225 - 2.360 GeV/c^2. The fit yields half-width-half-maximum 5.1 MeV/c^2 and has chi-squared per degree of freedom (χ^2/NDF) 19.6/20.

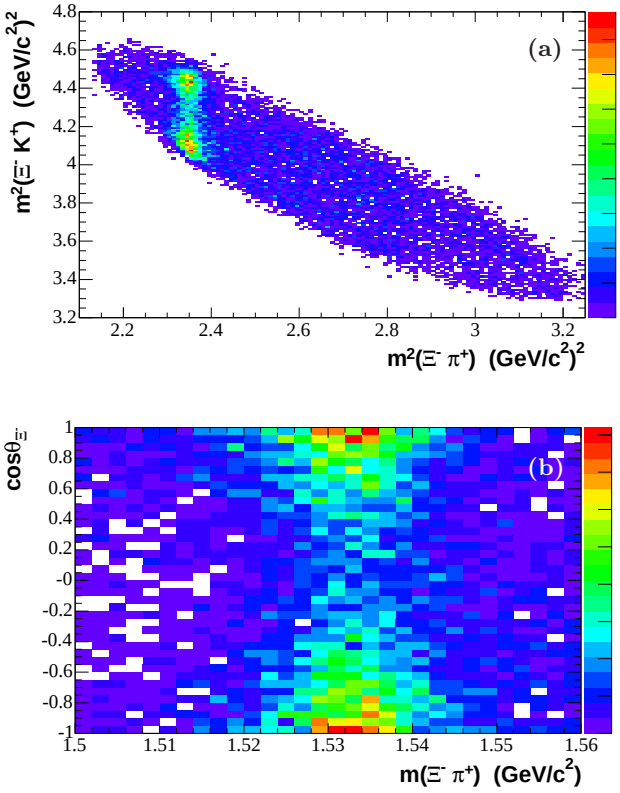

FIG. 2: (a) The Dalitz plot of $\Xi^- K^+$ versus $\Xi^- \pi^+$ invariant mass-squared for the Λ_c^+ signal region. (b) The corresponding rectangular Dalitz plot for the $\Xi(1530)^0$ mass region. (The online version of this figure is in color.)

III. $\Xi(1530)$ SPIN MEASUREMENT

The Dalitz plot for $\Lambda_c^+ \to \Xi^- \pi^+ K^+$ (Fig. 2) is dominated by the contribution from $\Lambda_c^+ \to \Xi(1530)^0 K^+$, where $\Xi(1530)^0 \to \Xi^- \pi^+$ is a strong decay. There is evidence for only one resonant structure, seen as the clear band at the nominal mass squared of the $\Xi(1530)^0$. The background events in the signal region of Fig.1(a) are represented by the events from the combined sideband regions indicated in this figure, which correspond to the same mass range [7]. A corrected distribution associated with the Λ_c^+ signal is obtained by subtraction (bin-by-bin) of the corresponding distribution for the sidebands from that for the signal region. This procedure is described as "sideband subtraction", and assumes linear mass dependence of the background. The sideband-subtracted projection of the $\Xi^- \pi^+$ invariant mass for the Λ_c^+ signal region of Fig. 1 (a) is shown in Fig. 1 (b).

The helicity formalism [8, 9] is applied to the quasi-two-body decay $\Lambda_c^+ \to K^+ \Xi(1530)^0$ in order to examine the implications of various $\Xi(1530)^0$ spin hypotheses for the angular distribution of the Ξ^- from $\Xi(1530)^0$ decay, under the assumption that the $\Xi(1530)^0$ mass region is dominated by a single spin state. As in Ref. [4], it is assumed that the spin of the charm baryon is 1/2. The choice of spin quantization axis along the direction of the $\Xi(1530)^0$ in the charm baryon rest-frame (r.f.) has the result that the $\Xi(1530)^0$ inherits the spin projection of the charm baryon, since any orbital angular momentum in the charm baryon decay has no projection in this direction. It follows that, regardless of the spin J of the $\Xi(1530)^0$, the density matrix which describes the $\Xi(1530)^0$ sample is diagonal, with non-zero values only for the $\pm 1/2$ spin projection elements, i.e., the helicity λ_i of the $\Xi(1530)^0$ can take only the values $\pm 1/2$. Since the final state Ξ^- and π^+ have spin values 1/2 and 0, respectively, the net final state helicity λ_f also can take only the values $\pm 1/2$. The helicity angle θ_{Ξ^-} is defined as the angle between the direction of the Ξ^- in the r.f. of the $\Xi(1530)^0$ and the quantization axis. Following the formalism of Ref. [4], the angular distribution of the Ξ^-

is then given by the total intensity,

$$I \propto \sum_{\lambda_i,\lambda_f} \rho_{i\,i} \left| A^J_{\lambda_f} D^{J\,*}_{\lambda_i\lambda_f}(\phi, \theta_{\Xi^-}, 0) \right|^2 , \qquad (1)$$

where the $\rho_{i\,i}$ ($i = \pm 1/2$) are the diagonal density matrix elements inherited from the charm baryon, and the sum is over all initial and final helicity states. The transition matrix element $A^J_{\lambda_f}$ represents the coupling of the $\Xi(1530)^0$ to the final state, $D^J_{\lambda_i\lambda_f}$ is an element of the Wigner rotation matrix [10], and the $*$ denotes complex conjugation. The resulting Ξ^- angular distribution integrated over ϕ is obtained for spin hypotheses

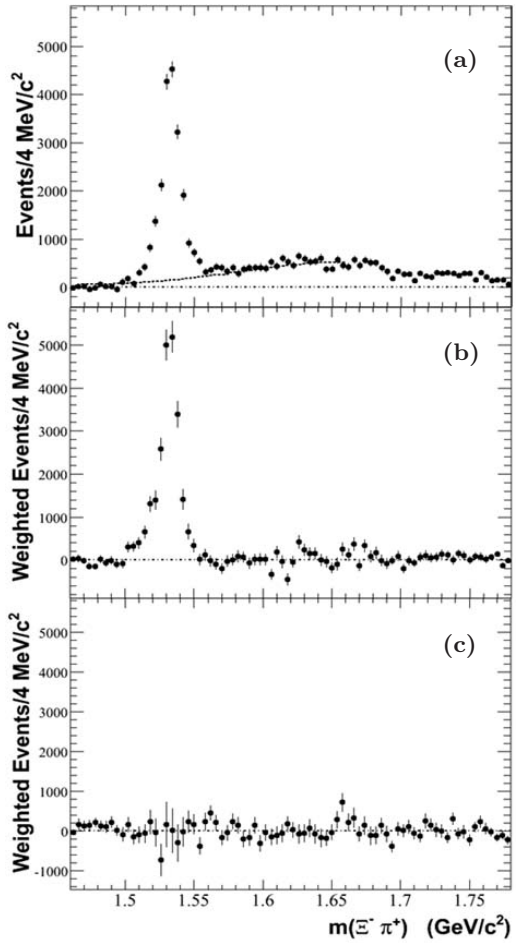

FIG. 3: The efficiency-corrected Λ_c^+-mass-sideband-subtracted (a) $\sqrt{2}P_0(\cos\theta_{\Xi^-})$, (b) $\sqrt{10}P_2(\cos\theta_{\Xi^-})$ and (c) $7/\sqrt{2}P_4(\cos\theta_{\Xi^-})$ moments of the $\Xi^-\pi^+$ system invariant mass distribution for the Λ_c^+ signal region. In (a) the dashed curve represents the estimated background contribution in the $\Xi(1530)$ region, obtained as described in the text.

$J_{\Xi(1530)} = 1/2$, $3/2$, and $5/2$, respectively, as follows:

$$dN/d\cos\theta_{\Xi^-} \propto\ 1 + \beta\cos\theta_{\Xi^-} \qquad (2)$$

$$dN/d\cos\theta_{\Xi^-} \propto\ 1 + 3\cos^2\theta_{\Xi^-} + \beta\cos\theta_{\Xi^-}(5 - 9\cos^2\theta_{\Xi^-}) \qquad (3)$$

$$dN/d\cos\theta_{\Xi^-} \propto\ 1 - 2\cos^2\theta_{\Xi^-} + 5\cos^4\theta_{\Xi^-} + \beta\cos\theta_{\Xi^-}(5 - 26\cos^2\theta_{\Xi^-} + 25\cos^4\theta_{\Xi^-}). \qquad (4)$$

The coefficient of the asymmetric term,

$$\beta = \left[\frac{\rho_{1/2\,1/2} - \rho_{-1/2\,-1/2}}{\rho_{1/2\,1/2} + \rho_{-1/2\,-1/2}}\right] \left[\frac{\left|A^J_{1/2}\right|^2 - \left|A^J_{-1/2}\right|^2}{\left|A^J_{1/2}\right|^2 + \left|A^J_{-1/2}\right|^2}\right],$$

is zero as a consequence of parity conservation in the strong decay of $\Xi(1530)^0$ to $\Xi^-\pi^+$, which implies $\left|A^J_{1/2}\right| = \left|A^J_{-1/2}\right|$. It should be noted that Eqs. 2-4 do not depend on any assumption as to the parity of the $\Xi(1530)$.

The normalized angular distribution of the Ξ^- obtained from Eq. 1, and expressed explicitly in Eqs. 2-4 for $J = 1/2, 3/2$ and $5/2$, respectively, can be written in general as

$$\frac{dN}{d\cos\theta_{\Xi^-}} = N\left[\sum_{l=0}^{l_{max}} \langle P_l\rangle P_l\left(\cos\theta_{\Xi^-}\right)\right], \qquad (5)$$

where $l_{max} = 2J - 1$, the value of each expansion coefficient $\langle P_l\rangle$ depends on J, and, if l is odd, $\langle P_l\rangle = 0$. The Legendre Polynomials satisfy

$$\int_{-1}^{1} d\cos\theta_{\Xi^-}\, P_i\left(\cos\theta_{\Xi^-}\right) P_j\left(\cos\theta_{\Xi^-}\right) = \delta_{i\,j}, \qquad (6)$$

(i.e., $P_l\left(\cos\theta\right) = \sqrt{2\pi}Y_l^0\left(\cos\theta, \phi\right)$, where Y_l^0 is a spherical harmonic function), so that

$$\int_{-1}^{1} \frac{dN}{d\cos\theta_{\Xi^-}} P_l\left(\cos\theta_{\Xi^-}\right) d\cos\theta_{\Xi^-} \ =\ N\langle P_l\rangle. \qquad (7)$$

For a data distribution containing N events, the left-hand side of Eq. 7 is approximately equal to

$$\sum_{k=1}^{N} P_l\left(\cos\theta^k_{\Xi^-}\right),$$

since for large N, the sum over the observed events provides a good approximation to the integral; throughout this paper, this summation is termed "the $P_l(\cos\theta_{\Xi^-})$ moment" or simply 'the P_l moment" of the data. Each assumption for J defines l_{max}, so that $\langle P_l\rangle = 0$ for $l > l_{max}$ and the $\langle P_l\rangle$ are calculable. For $J = 1/2, 3/2, 5/2$, $l_{max} = 0, 2, 4$, with the corresponding $\langle P_{l_{max}}\rangle$ values $1/\sqrt{2}$, $1/\sqrt{10}$ and $\sqrt{2}/7$, respectively. The relation

$$\sum_{k=1}^{N} \frac{P_{l_{max}}\left(\cos\theta^k_{\Xi^-}\right)}{\langle P_{l_{max}}\rangle} \approx N \qquad (8)$$

implies that the number of $\Xi(1530)^0$ signal events in a given mass interval is well-approximated if each event k is given weight

$$w_k = \frac{P_{l_{max}}\left(\cos\theta^k_{\Xi^-}\right)}{\langle P_{l_{max}}\rangle}, \qquad (9)$$

after efficiency correction [11] and background subtraction.

Since the angular distribution shown in Fig. 2(b) is clearly not flat, $\Xi(1530)$ spin 1/2 is ruled out. In order to test the $J = 3/2$ (5/2) hypothesis, each event is given a weight $w_k = \sqrt{10}P_2(\cos\theta^k_{\Xi^-})$ ($\frac{7}{\sqrt{2}}P_4(\cos\theta^k_{\Xi^-})$). Figure 3(a) shows the distribution of the $\sqrt{2}P_0(\cos\theta_{\Xi^-})$ moment which is just the efficiency-corrected distribution corresponding to Fig. 1(b) (the average efficiency is $\sim$ 27%). The $\sqrt{10}P_2(\cos\theta_{\Xi^-})$ and $7/\sqrt{2}P_4(\cos\theta_{\Xi^-})$ moments are shown in Figs. 3(b) and 3(c), respectively. Figure 3(b) indicates that spin 3/2 is strongly favored, as essentially all of the $\Xi(1530)$ signal is retained. In contrast, the $7/\sqrt{2}P_4(\cos\theta_{\Xi^-})$ moment shown in Fig. 3(c) is consistent with zero in the $\Xi(1530)$ signal region, so that spin 5/2 is clearly ruled out. The results for $l_{max} \geq 6$ (not shown) are similar to those of Fig 3(c). In order to quantify these results, the region $1.50 \leq m(\Xi^-\pi^+) \leq 1.65$ GeV/c^2 is defined as the $\Xi(1530)$ signal region. The dashed curve of Fig. 3(a) corresponds to a fit to the region $m(\Xi^-\pi^+) \leq 1.66$ GeV/c^2 with the signal region excluded; the fit function is a third order polynomial multiplied by phase space. This yields an estimated signal of 19159 ± 581 events. For Figs. 3(b) and (c), the moment sums for the signal region are 23355 ± 894 and 78 ± 1410, respectively. Clearly, $J = 3/2$ is the only viable $\Xi(1530)$ spin value. It follows that, based on the results of Refs. [2, 3] (i.e., $J^P = 3/2^+$ or $J^P = 5/2^-$), the present analysis, which shows that $J = 3/2$, also establishes positive parity, and that the $\Xi^-\pi^+$ system which results from the decay is in a P-wave orbital angular momentum state. Here, and in Refs. [2, 3], it is assumed that the Ξ^- has positive parity [1].

IV. THE $\Xi(1530)$ MASS REGION

Although Fig. 3 clearly establishes spin 3/2 for the $\Xi(1530)$, the analysis of the $\Xi^-\pi^+$ system described in the remainder of this paper indicates that a detailed understanding of the data is much less straightforward than Fig. 3 might indicate. If the momentum of the Ξ^- in the $\Xi^-\pi^+$ r.f. is denoted by q, a Breit-Wigner (BW) amplitude corresponding to orbital angular momentum L should be proportional to the centrifugal barrier factor q^L [12]. The lineshape for a $\Xi^-\pi^+$ P-wave BW should then be skewed toward high mass values. However, the distribution of Fig. 3(b), which should represent the square of a P-wave amplitude, appears to be skewed toward low mass values, in contradiction of this expectation. Furthermore, if the distribution in Fig. 3(a) is considered to represent a sum of squares of $\Xi^-\pi^+$ amplitudes, for which that in Fig. 3(b) represents the $J = 3/2$ contribution, their difference would be expected to behave like the background distribution in Fig. 3(a) in the $\Xi(1530)^0$ region. However, the $\Xi(1530)$ signal in Fig. 3(b) contains $\sim$ 4000 events more than that in Fig. 3(a), as indicated above, so that when the former is subtracted from the latter, the residual distribution exhibits a strong dip in the $\Xi(1530)$ region, and even reaches negative values. This behavior is clearly at odds with a simple interpretation of these distributions.

Moreover, the $\cos\theta_{\Xi^-}$ distribution in the $\Xi(1530)^0$ signal region indicates that a description in terms of a single $\Xi^-\pi^+$ amplitude corresponding to a resonant structure is an over-simplification. The Λ_c^+ mass-sideband-subtracted $\cos\theta_{\Xi^-}$ distribution for the $\Xi(1530)^0$ signal region (Fig. 4) exhibits a predominantly quadratic behavior, which indicates clearly that the spin of the $\Xi(1530)$ is not 1/2. A function $\propto \left(1 + 3\cos^2\theta\right)$ (solid curve of Fig. 4(b), the parametrization of Eq. 3) which corresponds to $J = 3/2$ for the $\Xi(1530)^0$ fits the data best, although there are clear deviations from the curve, and the fit confidence level (c.l.) is only 0.0003. The fit with the

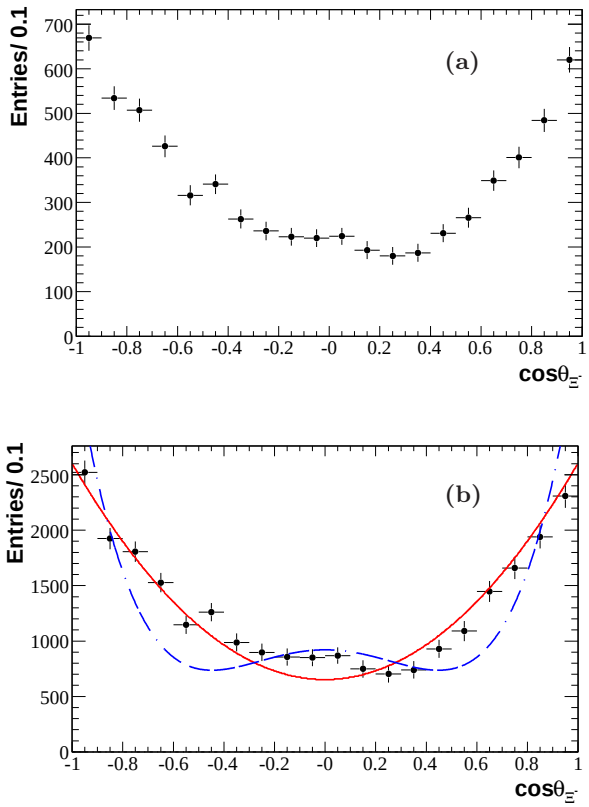

FIG. 4: The $\cos\theta_{\Xi^-}$ distribution for $\Lambda_c^+ \to \Xi^-\pi^+K^+$ data in the $\Xi(1530)^0 \to \Xi^-\pi^+$ signal region (a) before, and (b) after, efficiency correction. The solid (dashed) curve corresponds to the parametrization of the $\Xi(1530)$ angular distribution for the assumption of *pure* spin 3/2 (5/2).

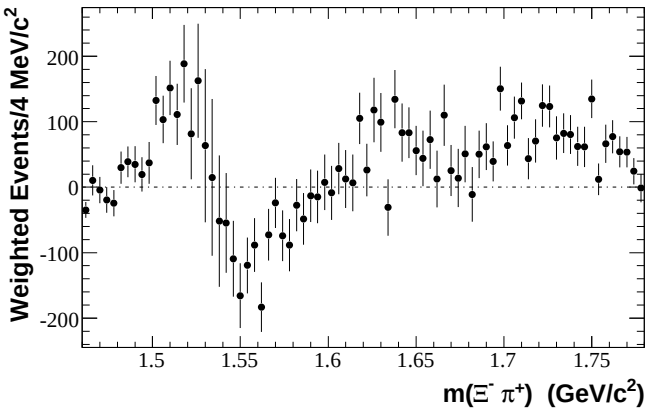

FIG. 5: The efficiency-corrected $P_1(\cos\theta_{\Xi^-})$ moment of the $\Xi^-\pi^+$ system invariant mass distribution corresponding to the Λ_c^+ signal region. The distributions for the sideband regions are consistent with zero, and so are not subtracted.

parametrization which corresponds to $J = 5/2$ (dashed curve, Eq. 4) is extremely poor, with c.l. 6×10^{-44}, as would be expected from the projection of Fig. 3(c). In addition, the distribution of Fig. 4(b) exhibits signs of forward-backward asymmetry.

The above symptoms indicate that a more complicated description is required if a quantitative understanding of the $\Xi^-\pi^+$ system is to be achieved.

Strong interactions in the $\Xi^-\pi^+$ system may give rise to interference between the resonant P-wave $\Xi(1530)$ amplitude and other $\Xi^-\pi^+$ amplitudes. Evidence for interference is seen in the behavior of the $P_1(\cos\theta_{\Xi^-})$ moment of the $\Xi^-\pi^+$ system as a function of invariant mass. The distribution shown in Fig. 5 is consistent with the interference pattern resulting from the rapid oscillation due to $\Xi(1530)$ P-wave BW phase motion in the presence of an amplitude with small slowly varying relative phase; the projection would then approximate the real part of the BW amplitude, as observed.

The oscillatory pattern seen in Fig. 5 is not observed for the high and low Λ_c^+ mass sideband regions, which confirms that the pattern is indeed due to $\Xi(1530)$ phase-motion in events produced from signal Λ_c^+ candidates, and is not simply an artifact of combinatorial background. As mentioned above, the $P_1(\cos\theta_{\Xi^-})$ moment for $m(\Xi^-\pi^+) < 1.58$ GeV/c^2 behaves very much like the real part of the $\Xi(1530)$ BW amplitude, which suggests that the phase of the amplitude yielding the interference effect is close to zero. The proximity of $\Xi^-\pi^+$ threshold, and the fact that the interference is seen in the $P_1(\cos\theta_{\Xi^-})$ moment, suggest that the effect is due primarily to the presence of an S-wave $\Xi^-\pi^+$ amplitude.

If it is assumed that only total spin J=1/2 and 3/2 amplitudes contribute, and if the description is restricted to S, P and D waves, the following angular distribution for the Ξ^- produced in $\Xi^-\pi^+$ decay is obtained:

$$\begin{aligned}\frac{dN}{d\cos\theta_{\Xi^-}} &= \left[\frac{1}{2}|S^{1/2}|^2 + |P^{3/2}|^2\left(\frac{1+3\cos^2\theta_{\Xi^-}}{4}\right)\right. \\ &+ \left.\sqrt{2}Re\left(S^{1/2}P^{3/2*}\right)\cos\theta_{\Xi^-}\right] \\ &+ \left[\frac{1}{2}|P^{1/2}|^2 + |D^{3/2}|^2\left(\frac{1+3\cos^2\theta_{\Xi^-}}{4}\right)\right. \\ &+ \left.\sqrt{2}Re\left(P^{1/2}D^{3/2*}\right)\cos\theta_{\Xi^-}\right] \qquad (10)\end{aligned}$$

where the amplitude notation is L^J.

The angular structure associated with the $J = L+1/2$ terms (Eq. 10, first bracket) is identical to that associated with the $J = L-1/2$ terms (Eq. 10, second bracket), i.e., there is a Minami ambiguity [13]. It follows that there are more unknown quantities than measurables, so that a complete set of amplitudes cannot be extracted from the data. However, since the $\Xi(1530)$ is a $P^{3/2}$ resonance, it is reasonable to attribute the $P_1(\cos\theta_{\Xi^-})$ moment behavior of Fig. 5 to the $S^{1/2}$-$P^{3/2}$ interference term of Eq. 10; in addition, D-wave amplitudes would not be expected to be significant for $\Xi^-\pi^+$ mass values close to threshold, so that a simple model which incorporates only $S^{1/2}$ and $P^{3/2}$ amplitudes might describe the data. This would imply that the intensity distribution of Fig. 3(b) corresponds to $|P^{3/2}|^2$ only. However, as discussed above, the difference in the distributions of Figs. 3(a) and (b) dips strongly in the $\Xi(1530)$ region, even reaching negative values, and so cannot be described by $|S^{1/2}|^2$. This indicates that the data in the $\Xi(1530)$ mass region require a more complicated explanation.

V. THE $\Xi^-\pi^+$ SYSTEM AT HIGHER MASS

The inclusion of a $D^{3/2}$ contribution (Eq. 10) does not solve the problem of the $\Xi(1530)$ mass region described at the end of Section IV, since Fig. 3(b) then corresponds to $|P^{3/2}|^2 + |D^{3/2}|^2$ and Fig. 3(a) to $|S^{1/2}|^2 + |P^{3/2}|^2 + |D^{3/2}|^2$. If the model is extended to include a $D^{5/2}$ amplitude, the Legendre Polynomial moments, P_0–P_4, are

expressed in terms of the amplitudes as follows:

$$P_0 = \frac{1}{\sqrt{2}}\left[\left|S^{1/2}\right|^2 + \left|P^{1/2}\right|^2 + \left|P^{3/2}\right|^2 + \left|D^{3/2}\right|^2 + \left|D^{5/2}\right|^2\right] \quad (11)$$

$$P_1 = \frac{2}{\sqrt{3}}\left[Re\left(S^{1/2}P^{3/2\,*}\right) + Re\left(P^{1/2}D^{3/2\,*}\right)\right] + \frac{6}{5}Re\left(P^{3/2}D^{5/2\,*}\right) \quad (12)$$

$$P_2 = \frac{1}{\sqrt{10}}\left[\left|P^{3/2}\right|^2 + \left|D^{3/2}\right|^2 + \frac{8}{7}\left|D^{5/2}\right|^2 + \sqrt{20}Re\left(S^{1/2}D^{5/2\,*}\right)\right] \quad (13)$$

$$P_3 = \frac{4}{5}\sqrt{\frac{3}{7}}Re\left(P^{3/2}D^{5/2\,*}\right) \quad (14)$$

$$P_4 = \frac{\sqrt{2}}{7}\left|D^{5/2}\right|^2 \quad (15)$$

These five equations involve nine unknown quantities (five amplitude magnitudes and four relative phase angles), and so cannot be solved. Additional input from polarization moments is required. Such an analysis is beyond the scope of the present paper. If we assume that the $P^{1/2}$ and $D^{3/2}$ amplitudes can be ignored, Eqs. 11-15 can be solved in principle. However, as is discussed below, even such a simplified model encounters difficulties in the $\Xi(1530)$ region.

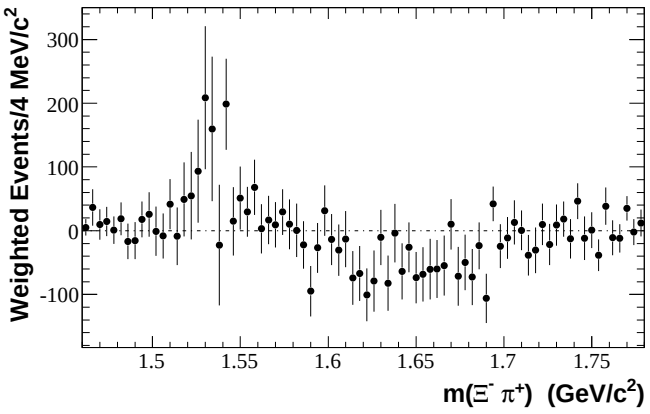

FIG. 6: The efficiency-corrected $P_3(\cos\theta_{\Xi^-})$ moment of the $\Xi^-\pi^+$ invariant mass distribution for the Λ_c^+ signal region. The distributions for the sideband regions are consistent with zero, and so are not subtracted.

In the context of this model, the absence of any significant P_4 moment in Fig. 3(c) indicates via Eq. 15 that $|D^{5/2}|$ must be small. However, since $P^{3/2}$ is large, $P^{3/2} - D^{5/2}$ interference might be seen in the mass-dependence of the P_3 moment (Eq. 14). This is shown in Fig. 6, where small, but significant, deviations from zero are in fact observed. Since there is a $P^{3/2} - D^{5/2}$ interference contribution to Eq. 12, an improved measure of the mass dependence of $S^{1/2} - P^{3/2}$ interference is obtained by subtracting $(\sqrt{21}/2)P_3$ from P_1. The $P_1 - (\sqrt{21}/2)P_3$ distribution is shown in Fig. 7, and the dip in the mass region $1.63 - 1.70$ GeV/c^2 of Fig. 5 has been removed by this procedure. Before the $\Xi(1530)$ region is examined in more detail, the behavior of $P_1 - (\sqrt{21}/2)P_3$ is considered in the mass region above ~ 1.6 GeV/c^2.

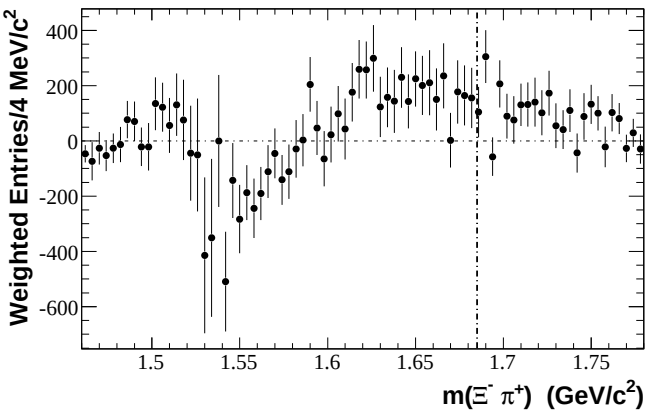

FIG. 7: The efficiency-corrected $P_1 - (\sqrt{21}/2)P_3$ moment of the $\Xi^-\pi^+$ system invariant mass distribution, corresponding to the Λ_c^+ signal region. The dot-dashed line indicates the $\Xi(1690)^0$ mass value [1]. The distributions for the sideband regions are consistent with zero, and so are not subtracted.

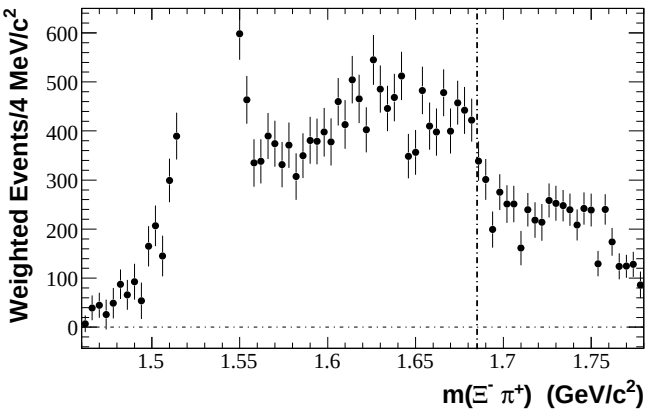

FIG. 8: The efficiency-corrected Λ_c^+ mass-sideband-subtracted $P_0(\cos\theta_{\Xi^-})$ moment of the $\Xi^-\pi^+$ system invariant mass distribution for the Λ_c^+ signal region (the distribution of Fig. 3(a) with the $\Xi(1530)$ region suppressed). The vertical dot-dashed line indicates the $\Xi(1690)^0$ mass value [1].

It is interesting to consider this in comparison to the distribution of Fig. 3(a) with the $\Xi(1530)$ region sup-

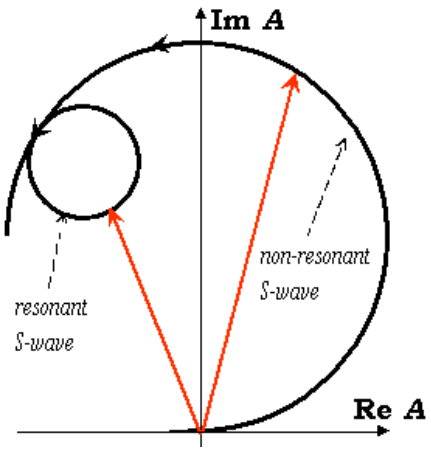

FIG. 9: A cartoon of an Argand diagram which illustrates a possible cause for the dip in the $\Xi^-\pi^+$ invariant mass distribution due to the presence of the $\Xi(1690)^0 \to \Xi^-\pi^+$.

pressed (Fig. 8), which shows a significant decrease in intensity at $\sim$ 1.7 GeV/c^2. As mentioned previously, the behavior of the P_1 moment in the $\Xi(1530)$ region indicates a small $S^{1/2}$ amplitude with phase $\sim$ 0 deg. relative to the $P^{3/2}$ amplitude in order that P_1 closely resemble the real part of the $\Xi(1530)$ BW amplitude. If the $S^{1/2}$ amplitude did not change significantly at higher mass values, the BW amplitude would cause P_1 to approach zero from below with increasing mass. Instead, P_1 passes through zero at $\sim$ 1.6 GeV/c^2 and remains positive thereafter (Fig. 7). Since P_1 represents the projection of the $S^{1/2}$ amplitude onto the $P^{3/2}$ amplitude, this means that the $S^{1/2}$ phase is increasing significantly, is only 90 deg. behind the $P^{3/2}$ phase at $\sim$ 1.6 GeV/c^2 where P_1 is $\sim$ 0, and continues to increase at higher mass. The dip in the mass distribution of Fig. 8 is in the vicinity of the $\Xi(1690)$, which is known to have a small coupling to $\Xi^-\pi^+$ [14]. This dip could occur as the result of the coherent addition of a small, resonant $\Xi(1690)$ amplitude to the slowly increasing $S^{1/2}$ amplitude, as shown schematically by the cartoon of Fig. 9. Here the large circle represents a slowly-varying non-resonant $S^{1/2}$ amplitude for which the phase reaches 90 deg. at mass $\sim$ 1.6 GeV/c^2, relative to a $P^{3/2}$ amplitude; the latter should be approximately aligned with the negative real axis at this mass value. As the phase increases beyond 90 deg., the $S^{1/2}$ projection on the $P^{3/2}$ amplitude [i.e., P_1] will increase as seen in Fig. 7. The small circle represents the subsequent coherent addition of a small resonant $\Xi(1690)$ amplitude. The resultant amplitude will then yield a dip in overall intensity in the $\Xi(1690)$ region with very little effect on the phase, and hence on P_1 (cf. Fig. 7). The inference which can be drawn is that the $\Xi(1690)$ decays strongly to the $\Xi^-\pi^+$ system in an S-wave orbital state, and hence that it has spin-parity $1/2^-$. As such, this represents the first experimental information on the spin-parity of the $\Xi(1690)$. Spin 1/2 is favored also by an analysis of the Dalitz plot corresponding to the decay process $\Lambda_c^+ \to \Lambda\bar{K}^0K^+$ [15].

The behavior of the $S^{1/2}$ amplitude described above is remarkably similar to that obtained for the $I = 1/2$ S-wave $K^-\pi^+$ scattering amplitude in the LASS experiment [16]. There the slow, monotonic increase in the S-wave amplitude at low mass is described by an effective range parametrization. The phase reaches $\sim$ 90 deg. before the coherent addition of a resonant $K_0^*(1430)$ contribution takes effect, and the resultant amplitude decreases quickly almost to zero. The main difference in the $K^-\pi^+$ case is that the resultant amplitude remains elastic (within error) up to $K\eta'$ threshold, so that the decrease in S-wave intensity is quite substantial. Since the $\Xi(1690)$ decays significantly via modes other than $\Xi^-\pi^+$, a similar mechanism would be expected to yield less dramatic results, as is in fact observed in Fig. 8. This similarity between $K\pi$ and $\Xi\pi$ scattering amplitudes may be an example of the proposed effective supersymmetry between mesons and baryons involving the replacement of a light anti-quark in the meson by a light diquark to form the related baryon [17]. For $I = 1/2$, the amplitudes describing $K^-\pi^+$ scattering are the same as for $K^+\pi^-$, and similarly those describing $\Xi^-\pi^+$ scattering are proportional to those for $\Xi^0\pi^-$ scattering; $K^+\pi^-$ scattering is then converted to $\Xi^0\pi^-$ scattering by replacing the $\bar{s}$ quark in the K^+ with an (ss) diquark to obtain the Ξ^0. In Ref. [17], the effective symmetry is demonstrated by relating various baryon-baryon and meson-meson mass differences with impressive precision. It seems reasonable to conjecture that this symmetry might also be manifest in the dynamics of appropriately related meson-meson and baryon-meson scattering processes.

VI. THE $\Xi(1530)^0$ LINESHAPE

In the $\Xi(1530)$ region, $S^{1/2} - D^{5/2}$ interference does in fact contribute to the P_2 moment distribution in Fig. 3(b) (cf. Eq. 13), but not to the distribution in Fig. 3(a) (cf. Eq. 11), so that the $\Xi(1530)$ signal in Fig. 3(b) might be larger than that in Fig. 3(a). In addition, this contribution might distort the lineshape in Fig. 3(b), but should not affect that in Fig. 3(a), which is obtained by integration over $\cos\theta_{\Xi^-}$. In order to test this conjecture, fits to the distributions in Figs. 3(a) and 3(b) are performed in which the $\Xi(1530)$ lineshape is described by

$$\frac{dN}{dm} = C\frac{\left(p^{2L}/D_L(p,R)\right)\left(q^{2l}/D_l(q,R)\right)}{\left(m_0^2 - m^2\right)^2 + m_0^2\Gamma_{tot}(m)^2} p\cdot q, \quad (16)$$

where C is a constant, p is the momentum of the K^+ in the Λ_c^+ r.f., and q is the momentum of the Ξ^- in the $\Xi^-\pi^+$ r.f.; L is the orbital angular momentum in the Λ_c^+ decay ($L = 1$ is chosen), and l that in the $\Xi(1530)$ decay (for which $l = 1$); D_L, D_l are Blatt-Weisskopf barrier factors [12] with radius parameter R, and, for example, $D_1(q,R) = 1 + (qR)^2$; $R = 3$ GeV^{-1} ($\sim$ 0.6 f)

is chosen [16]. The $\Xi(1530)$ mass is m_0, and $\Gamma_{tot}(m)$ its mass-dependent total width, which consists of the sum of partial widths to $\Xi^0\pi^0$ and $\Xi^-\pi^+$. If the mass differences between these modes are ignored, the mass-dependent total width is then

$$\Gamma_{tot}(m) = \Gamma_0 \frac{q}{q_0} \frac{m_0}{m} \frac{q^2}{D_1(q,R)} \frac{D_1(q_0,R)}{q_0^2}, \qquad (17)$$

where Γ_0 is the width of the $\Xi(1530)$, and $q_0 = q(m_0)$. For the fits to the data of Fig. 3(a), an incoherent background function of the form

$$b = (p \cdot q) \sum_{i=0}^{3} c_i m^i \qquad (18)$$

is included also.

In each fit, the fit function is convolved with a mass resolution function consisting of two Gaussian distributions with a common center and fixed fractional contributions, but with r.m.s. deviation values which depend on $\Xi^-\pi^+$ invariant mass. For the resolution function, the resulting half-width-at-half-maximum increases from ~ 0.5 MeV/c^2 just above threshold, to ~ 1.5 MeV/c^2 at the $\Xi(1530)$, reaching ~ 2.5 MeV/c^2 at ~ 1.6 GeV/c^2, so that the resolution in the signal region is excellent. The degradation of the mass resolution with increasing $\Xi^-\pi^+$ mass should, if anything, cause the observed $\Xi(1530)^0$ lineshape to be slightly skewed toward high mass; it follows that this cannot be the source of the skewing of the lineshapes of Figs. 3(a) and 3(b) toward low mass. The convolution procedure takes quantitative account of the resolution behavior, but, since the resolution is excellent, this has little impact on the description of the data. The fit results with $\Xi(1530)^0$ mass and width fixed at their PDG values [1] are shown in Fig. 10. In Figs. 10(a) and 10(c), the dots represent the data of Figs. 3(a) and 3(b), respectively, while the histograms represent the mass-resolution-smeared fit functions integrated over the corresponding mass intervals. The fit residuals (data − histogram) are shown in Figs. 10(b) and 10(d), respectively. These show similar very large systematic deviations from zero, and the fits have correspondingly poor c.l. values (6×10^{-16} and ~ 0, respectively). With the mass and width parameters free in the fits, the c.l. values are still poor, and the values obtained differ significantly from the PDG values (e.g., $m_0 = 1534.4 \pm 0.1$ MeV/c^2 and $\Gamma_0 = 13.2 \pm 0.5$ MeV for Fig. 10(a)). If the Blatt-Weisskopf radius parameter is allowed to be free, an acceptable fit to the mass distribution is not obtained (c.l. $\sim 10^{-3}$), the residuals still show systematic deviations from zero, and the mass and width values obtained still differ significantly from their PDG values. Similarly, the fit to the P_2 moment mass dependence with mass, width and radius parameters free remains poor (c.l. $\sim 10^{-7}$); in addition, the radius parameter increases to ~ 100 GeV^{-1} (which is equivalent to the use of an S-wave Breit-Wigner) in an attempt to reproduce the observed lack of skewing toward high mass expected for a P-wave decay. Since the P-wave nature of the decay has been establised, this is certainly an unacceptable result.

As a check of the signal parametrization of Eq. 16, this function (with $R = 3$ GeV^{-1}) has been used in fits to the published $\Xi^-\pi^+$ mass distributions from four of the experiments [18–21] used to obtain the PDG mass and width values [1]. These are Hydrogen Bubble Chamber experiments, and each mass distribution is obtained as the projection of the Dalitz plot for the reaction $K^-p \to \Xi^-\pi^+K^0$ (Ref. [19] uses some additional contributions). The analysis samples are small (125, 350, 324, and 1313 events, respectively), and the details of the fit functions used in Refs. [18–21] are not made clear. It is found that the non-resonant background contributions are well-described using only the $(p \cdot q)$ phase space factor of Eq. 18, and Eq. 16, convolved with a Gaussian of r.m.s. deviation specified for each experiment, is used to represent the $\Xi(1530)$ signal. Good c.l. values are obtained, and the resulting weighted average mass (1532.2 ± 0.2 MeV/c^2) and width (9.9 ± 0.5 MeV) values agree well with those from the PDG [1]. This indicates that the choice of signal and background functions is not the reason for the poor-quality fits to the data of Fig. 10. Furthermore, since no significant improvement in fit quality is observed in going from the P_2 fit to the P_0 fit, it follows that the difficulty in fitting the former cannot be attributed to the presence of an $S^{1/2} - D^{5/2}$ interference contribution, since this would not be present for the latter.

This striking failure to describe the most obvious feature of the $\Xi^-\pi^+K^+$ Dalitz plot leads to the conclusion that a satisfactory description of the observed $(m(\Xi^-\pi^+), \cos\theta_{\Xi^-})$ distribution cannot be obtained in terms of amplitudes pertaining solely to the $\Xi^-\pi^+$ system. The difficulties probably result from overlap and interference effects involving amplitudes associated with the $K^+\pi^+$ and/or the Ξ^-K^+ systems (if the possibility of direct three-body decay is ignored). The $K^+\pi^+$ system has $I = 3/2$, and has been observed to have only an S-wave amplitude, which varies slowly with mass in the relevant region (≤ 1 GeV/c^2). It seems unlikely that such an amplitude could lead to significant distortion of the mass and $\cos\theta_{\Xi^-}$ dependences of the $\Xi^-\pi^+$ system, but the relevant quantitative analysis has not yet been attempted. In contrast, the Ξ^-K^+ system could have contributions from high-mass Λ or Σ^0 resonant structures in the region of overlap with the $\Xi(1530)$ (> 2 GeV/c^2, cf. Fig. 2(a)). Very little is known about such states or their couplings to Ξ^-K^+ [1], and there is no clear evidence for their presence in the Dalitz plots of Fig. 2. Indeed the only "evidence" for such contributions is the failure of the description of the $\Xi(1530)$ region solely in terms of $\Xi^-\pi^+$ amplitudes in the present analysis. This seeming impasse might benefit from analyses of related Λ_c^+ decay processes, such as $\Lambda_c^+ \to (\Lambda\eta)\pi^+$ or $\Lambda_c^+ \to (\Lambda\pi^0)\pi^+$, although these may suffer from their own particular complications related to other quasi-two-

body modes.

VII. CONCLUSION

In conclusion, the analysis of the Legendre Polynomial moments of the $\Xi^-\pi^+$ system which result from data on the decay $\Lambda_c^+ \to \Xi^-\pi^+K^+$ has established quite clearly, on the basis of Figs. 3 (b) and 3 (c), that the $\Xi(1530)$ hyperon resonance has spin 3/2. In conjunction with previous analyses [2, 3], this also definitively establishes positive parity, and hence that the $\Xi(1530)$ is a $P^{3/2}$ resonance. However, comparison of the $P_2(\cos\theta_{\Xi^-})$ moment to the $\Xi^-\pi^+$ mass distribution, and fits to the angular decay distribution in the $\Xi(1530)$ region, indicate that it is necessary to include other $\Xi^-\pi^+$ amplitudes in order to obtain a complete description of the data. In particular, the observation of a $P_1(\cos\theta_{\Xi^-})$ moment exhibiting oscillatory behavior in the $\Xi(1530)^0$ region indicates the need for an $S^{1/2}$ amplitude, while providing first evidence for the expected rapid BW phase motion of the $P^{3/2}$ $\Xi(1530)^0$ amplitude. However, a simple model incorporating only these amplitudes and a $D^{5/2}$ amplitude is ruled out because of the failure to describe the $\Xi(1530)^0$ lineshape. The presence of the $S^{1/2}$ amplitude at high mass, and the behavior of the mass distribution at ~ 1.7 GeV/c^2, suggest that a resonant $\Xi(1690)^0$ amplitude may be adding coherently to this amplitude, thus leading to the inference of spin-parity $1/2^-$ for the $\Xi(1690)$. It appears that a quantitative description of the $\Xi(1530)$ lineshape, and indeed of the entire Dalitz plot, must incorporate these features together with amplitude contributions associated with the $K^+\pi^+$ and/or the Ξ^-K^+ systems. An analysis of this complexity will be performed when the full *BABAR* data sample (integrated luminosity approximately 500 fb^{-1}) is available.

VIII. ACKNOWLEDGEMENTS

We are grateful for the extraordinary contributions of our PEP-II colleagues in achieving the excellent luminosity and machine conditions that have made this work possible. The success of this project also relies critically on the expertise and dedication of the computing organizations that support *BABAR*. The collaborating institutions wish to thank SLAC for its support and the kind hospitality extended to them. This work is supported by the US Department of Energy and National Science Foundation, the Natural Sciences and Engineering Research Council (Canada), the Commissariat à l'Energie Atomique and Institut National de Physique Nucléaire et de Physique des Particules (France), the Bundesministerium für Bildung und Forschung and Deutsche Forschungsgemeinschaft (Germany), the Istituto Nazionale di Fisica Nucleare (Italy), the Foundation for Fundamental Research on Matter (The Netherlands), the Research Council of Norway, the Ministry of Education and Science of the Russian Federation, Ministerio de Educación y Ciencia (Spain), and the Science and Technology Facilities Council (United Kingdom). Individuals have received support from the Marie-Curie IEF program (European Union) and the A. P. Sloan Foundation.

[1] W.-M. Yao *et al.* (PDG2006), J.Phys. G:Nucl.Part.Phys. **33**, 1 (2006).
[2] P. Schlein *et al.*, Phys. Rev. Lett. **11**, 167 (1963).
[3] J. Button-Shafer *et al.*, Phys. Rev. **142**, 883 (1966).
[4] The *BABAR* Collaboration, B. Aubert *et al.*, Phys. Rev. Lett. **97**, 112001 (2006).
[5] The use of charge conjugate reactions is implied throughout this paper.
[6] B. Aubert *et al.*, Nucl. Instr. Meth. **A479**, 1 (2002).
[7] The signal and low- and high-mass-sideband regions correspond to [2.265,2.307], and [2.223,2.244], [2.328,2.349] GeV/c^2, respectively.
[8] M. Jacob and G. C. Wick, Ann. Phys. **7**, 404 (1959).
[9] S. U. Chung, CERN Yellow Report, CERN 71-8 (1971).
[10] E. Wigner, *Gruppentheories*, Freidrich Vieweg und Sohn, Braunschweig (1931); *Group Theory*, Academic Press, New York (1959).
[11] Each selected event is weighted by the inverse value of its calculated efficiency, which is parametrized as a function of $\cos(\theta_{\Xi^-})$ and $m(\Xi^-\pi^+)$ using $\Lambda_c^+ \to \Xi^-\pi^+K^+$ signal Monte Carlo events.
[12] J. M. Blatt and V. F. Weisskopf, *Theoretical Nuclear Physics*, John Wiley and Sons (1952).
[13] S. Minami, Theor. Phys. **11**, 213 (1954).
[14] M.I. Adamovich *et al.*, Eur. Phys. J. **C5**, 621 (1998).
[15] Veronique Ziegler, *Ph.D. Thesis*, SLAC-R-868 (2007).
[16] D. Aston *et al.*, Nucl. Phys. **B296**, 493 (1988).
[17] M. Karliner and H. Lipkin, arXiv: hep-ph/0611306.
[18] G. W. London *et al.*, Phys. Rev. **143**, 1034 (1966).
[19] L. Kirsch *et al.*, Nucl. Phys. **B40**, 349 (1972).
[20] S. Borenstein *et al.*, Phys. Rev. **D5**, 1559 (1972).
[21] C. Baltay *et al.*, Phys. Lett. **42B**, 129 (1972).

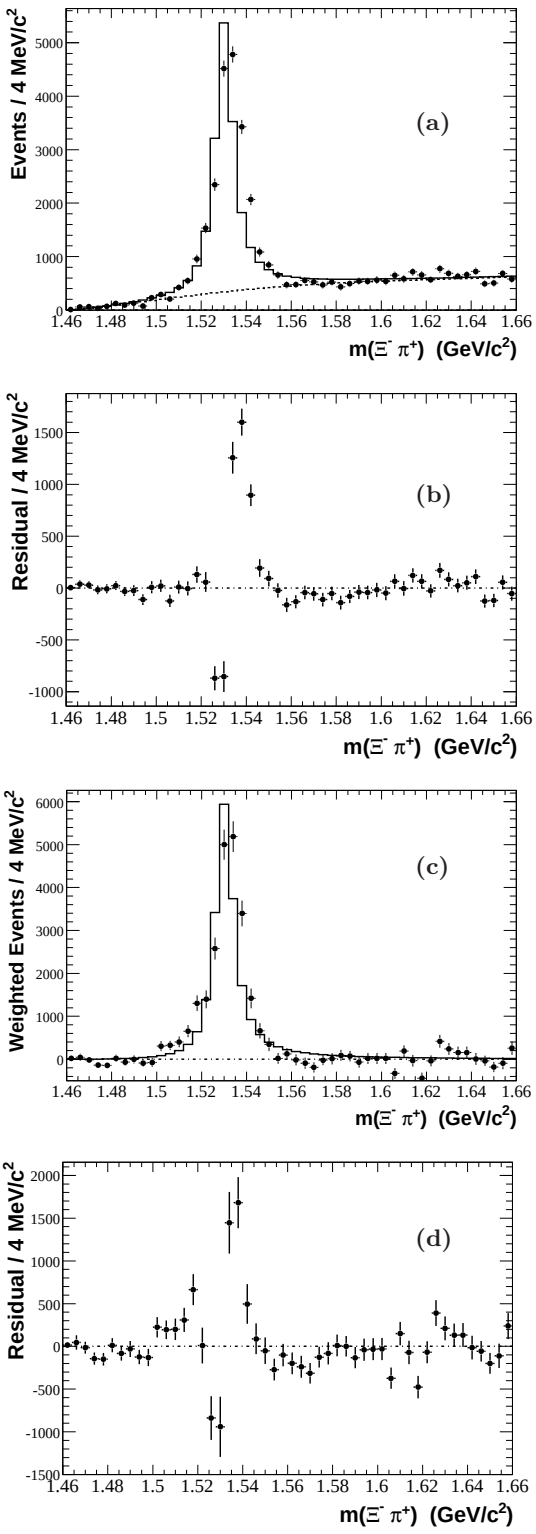

FIG. 10: The efficiency-corrected Λ_c^+-mass-sideband-subtracted (a) $\sqrt{2}P_0(\cos\theta_{\Xi^-})$ and (c) $\sqrt{10}P_2(\cos\theta_{\Xi^-})$ moment distributions for the $\Xi^-\pi^+$ system, for the Λ_c^+ signal region (solid dots). The fits represented by the histograms are described in the text. In (b) [(d)] the difference between the data points and the histogram in (a) [(c)] is shown.